Geotechnical Aspects of Underground Construction in Soft Ground – Viggiani (ed)
© 2012 Taylor & Francis Group, London, ISBN 978-0-415-68367-8

Centrifuge modelling of the response of buildings to tunnelling

R.P. Farrell
Laing O'Rourke (formerly University of Cambridge), UK

R.J. Mair
Department of Engineering, University of Cambridge, UK

ABSTRACT: Understanding how buildings respond to tunnelling induced ground movements is an area of great importance for many urban tunnelling projects. Testing described in this paper aims to investigate soil structure interaction effects by observing the response of elastic and non elastic beams of varying stiffness and geometry to tunnelling, using the 8 m diameter beam centrifuge at Cambridge University. Soil and structure displacements are extensively monitored through a photo imaging technique which enables a detailed analysis of the interaction mechanisms. Results demonstrate that buildings can significantly modify greenfield ground movements in both the vertical and horizontal planes. The magnitude of the modification is shown to be strongly dependent on the relative building stiffness. It is also shown that negligible horizontal strains are transferred into the model buildings. This can have significant implications for commonly adopted damage assessment methods.

1 INTRODUCTION

While relatively accurate predictions of the greenfield ground movements, in both the vertical and horizontal planes, can be made (Mair & Taylor, 1997), the presence of a structure alters these movements in what is termed soil-structure interaction. The estimation of the risk of damage to buildings, however, typically involves assuming that the structure deforms according to the greenfield ground movements. Estimates of the damage using this assumption can therefore be highly conservative.

Potts & Addenbrooke (1997) conducted a parametric finite element analysis investigating the response of buildings to tunnelling. Two parameters were defined to explain the modification to the settlement and axial response of buildings; these were the relative bending stiffness (ρ^*) and the relative axial stiffness (α^*). ρ^* and α^* were later modified by Franzius et al (2006), the former to be dimensionless. Expressions for ρ^*_{mod} and α^*_{mod} are presented in Equations 1 and 2 respectively:

$$\rho^*_{mod} = \frac{EI}{E_s B^2 z_0 L} \quad (1)$$

$$\alpha^*_{mod} = \frac{EA}{E_s BL} \quad (2)$$

where EI and EA are the bending stiffness and the axial stiffness of the structure respectively. E_s is the secant stiffness of the soil at 0.01% axial strain, at a depth of $z = z_0/2$. B is the building width and L is the length parallel to the tunnel heading. Dimensions are illustrated in Figure 1.

Settlement distortions to buildings are typically measured in both hogging and sagging modes of deformation using the deflection ratio (Δ/L or DR, defined in Figure 1). The hogging and sagging regions are partitioned by the point of inflexion (i) of the settlement trough. Potts and Addenbrooke (1997) quantified the modification to settlement distortions in terms of the ratio of the measured deflection ratio to the equivalent greenfield value, as presented in Equation 3. This ratio is given the term 'modification factor' (M^{DRhog} and M^{DRsag}).

$$M^{DR} = \frac{DR^{str}}{DR^{GF}} \quad (3)$$

Where DR^{GF} is the greenfield deflection ratio and DR^{str} is the deflection ratio displayed by the building; both are defined separately in hogging and sagging.

Modification factors to the greenfield settlement distortions are highly dependent on ρ^*_{mod} (Franzius et al., 2006). Similarly, the modification to tensile and compressive horizontal strains, in the hogging and sagging regions respectively, are highly dependent on α^*_{mod} (Franzius et al., 2006).

This paper presents the results of a series of centrifuge tests in which model aluminium, masonry

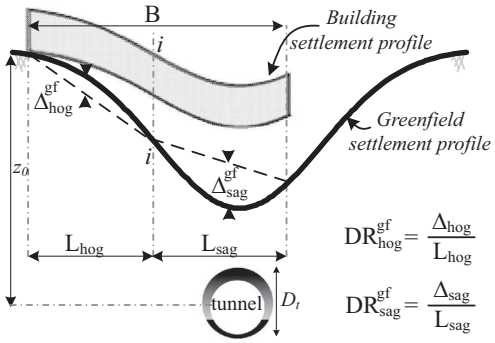

Figure 1. Influence of soil-structure interaction on settlement distortions.

and micro-concrete beam structures of varying stiffness and geometry are subjected to tunnelling induced ground movements. A greenfield test was also carried out, the results of which are used to quantify the modification to greenfield distortions that the various buildings display.

2 EXPERIMENTAL SETUP

2.1 *Centrifuge package and model design*

A series of centrifuge tests were carried out on the 8 m diameter centrifuge at the University of Cambridge to investigate the response of buildings to tunnelling in sands. Figure 2 shows the package used for this series of tests.

Centrifuge tests were carried out under plane strain conditions at 75 g. Using common scaling laws (Taylor, 1995), the model was designed to represent a 6.15 m diameter (D) tunnel with cover (C) of 8.25 m (at prototype scale), in fraction E silica sand. Model dimensions are shown in Figure 3.

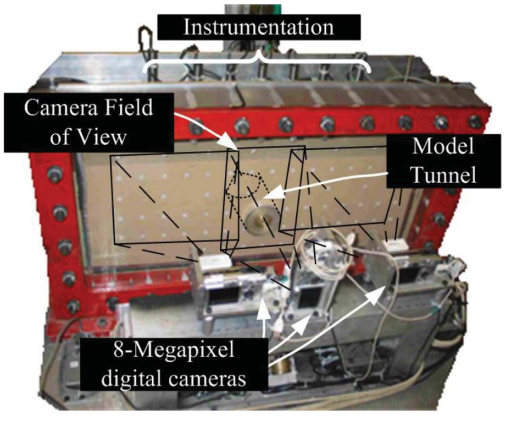

Figure 2. Centrifuge model package.

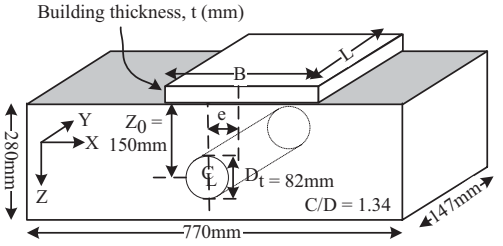

Figure 3. Model dimensions (in model scale).

Sand was poured into the model using an automatic sand pourer which enables a high level of repeatability between tests to be achieved. The model was poured with the Perspex face down and with the model tunnel in place, allowing for a uniform distribution of sand throughout the entire model. Relative sand density was 90% for this series of tests.

The model tunnel was formed using a brass mandrill with an outer latex rubber lining. The resulting annulus between the two is filled with water until an 82 mm diameter cylinder is obtained. This model tunnel is then placed in a recess in the front Perspex face and the back aluminium plate to achieve plane strain conditions.

During the test, volume losses are imposed by withdrawing the fluid from the tunnel using a piston and motor driven actuator system. This system is calibrated to withdraw the water at a controlled rate. The volume loss is determined from the ratio of the volume of fluid withdrawn to the volume of the tunnel. This method allows the volume loss to be accurately determined throughout the test.

To avoid volume changes in the tunnel as the model spins up to 75 g, due to remaining air in the system, the tunnel-piston system is connected to a fixed head of water in a standpipe at the back of the model. The resulting pressure head at the tunnel axis corresponds to the vertical total stress at the tunnel axis. The connection to the standpipe is controlled remotely using a solenoid valve and is opened during spin-up, and closed again once the model reaches 75 g, before initiating volume losses.

The face of the package was formed from Perspex to allow the use of particle image velocimetry (PIV) (White et al, 2003) to measure soil displacements. This technique uses digital imaging to track the movements of patches of pixels throughout the test. As PIV tracks the inherent soil texture, intrusive markers are not required. For this purpose, three 8 megapixel cameras were mounted on the front of the package (see Figure 2). Volume losses were induced in 0.1% increments and digital photos taken at each increment. This allows the measured displacements to be related to a specific volume loss.

2.2 *Modelling of buildings*

Two different types of building were considered in this research, namely fully elastic beam structures and beam structures capable of cracking.

Fully elastic structures used in this series of tests were constructed from aluminium beams (E = 70GPa) of varying thickness. The width of each aluminium beam was kept constant throughout the test series (B = 400 mm) and each structure was placed symmetrically about the tunnel axis. In each case plane strain conditions were present. A rough interface was modelled by gluing fraction E sand to the base of the structure. Geometric and structural properties for each of the 4 no. aluminium beams tested (STR-1 to STR-4) are given in Table 1.

Beam buildings capable of cracking were modelled using micro concrete and masonry with cement based mortar. Micro concrete mixes were formed from Orindary Portland Cement (OPC) and various grades of relatively fine sand (fraction C, D and E represent 45%, 30% and 25% of the aggregate mix respectively). The stiffness of the mix at various water-cement ratios (w/c) was calibrated using point load tests on sacrificial model beams. This also allowed for the effect of time on the mix strength to be assessed. The Young's modulus (E) of the micro-concrete mix at the w/c ratio of 0.8, used in test MCS-1, was estimated as 4 GPa at the time of testing.

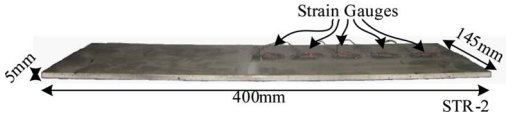

Figure 4. Model aluminium beam building (STR-2) with strain gauges.

Masonry buildings were modelled using 1/12th scale model bricks with an OPC based mortar. Plaster of Paris was added to the mortar to reduce the ductility and model the characteristics of real masonry more accurately. Point load tests on sample masonry walls indicated a Young's modulus (E) of 1.5–2GPa for the 2 no. masonry buildings modelled in this series of tests, MAS-1 (see Figure 5a) and MAS-2L. A further masonry building, termed MAS-2R, was modelling using 1/50th scale model bricks with an elastic silica gel mortar (see Figure 5b) to simulate a beam with a very low bending and axial stiffness. Geometric and structural properties for each of beams tested are given in Table 1.

Prototype scale axial (EA) and bending (EI) stiffness values modelled are comparable with values from similar centrifuge studies and from estimates of the stiffness of actual structures from case studies (see Figure 6). The influence of building weight was not investigated in this test series. Model structures were also fitted with strain gauges to measure the bending and horizontal strains at various locations. An indication of the contact stress between buildings and the soil was obtained from Earth

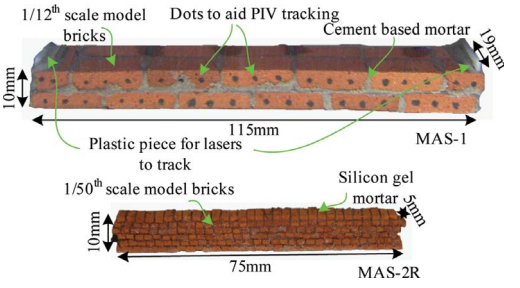

Figure 5. Model masonry buildings with (a) cement based mortar and (b) silica gel mortar.

Table 1. Test series details.

Test Name	Material	Model scale B (mm)	e[†1] (mm)	t (mm)	L (mm)	EI (kNm²/m)	EA (kN/m)	Prototype scale EI (kNm²/m)	EA (kN/m)
GF-1	Greenfield—no building								
STR-1	Aluminium	400	0	1.6	145	2.4×10^{-2}	1.1×10^{5}	1×10^{2}	8.4×10^{6}
STR-2	Aluminium	400	0	5	145	7.3×10^{-1}	3.5×10^{5}	3.1×10^{5}	2.6×10^{4}
STR-3	Aluminium	400	0	10	145	5.8×10^{0}	7×10^{5}	2.5×10^{6}	5.3×10^{7}
STR-4	Aluminium	400	0	20	145	4.7×10^{1}	1.4×10^{6}	2.0×10^{7}	1.0×10^{8}
MCS-1	Micro-concrete	400	0	5	145	4.1×10^{-2}	2.0×10^{4}	1.8×10^{4}	1.5×10^{6}
MAS-1	Masonry	115	–67	10	18	1.6×10^{-1}	2.0×10^{4}	7.1×10^{4}	1.5×10^{6}
MAS-2	(a)Masonry[†2]	195	–45	10	18	1.25×10^{-1}	1.5×10^{4}	5.4×10^{4}	1.1×10^{6}
MAS-2	(b)Masonry[†2]	75	120	10	5	1.25×10^{-2}	1.5×10^{3}	5.4×10^{3}	1.1×10^{5}

[†1]where, e is the eccentricity of the building measured as the distance from the mid-point of the building to the tunnel centreline.

[†2] two buildings were tested in MAS-2. Building (a), MAS-2L, was located to the left of the tunnel and building (b), MAS-2R, was located to the right hand side of the tunnel.

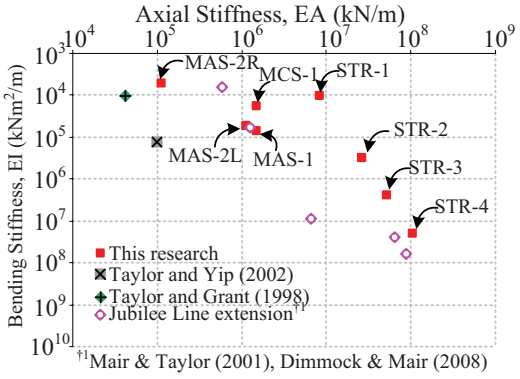

Figure 6. Bending and axial stiffness of real structures.

Pressure Cells (EPC's) which were glued to the underside of model buildings.

Similar modelling techniques have been adopted by Taylor & Grant (1998) and Marshall (2009) in centrifuge modelling of the response to tunnelling of structures and pipelines respectively.

3 BUILDING SETTLEMENT RESPONSE

3.1 *Building settlements*

The settlement profiles of the aluminium beam buildings, STR-1 to STR-4, at 2% volume loss are illustrated in Figure 7. The greenfield settlement profile (GF-1) is also shown for reference STR-1 is seen to behave fully flexibly with regions of hogging and sagging evident, while STR-4 demonstrates the most rigid response. Therefore, depending on a building's stiffness, or more specifically ρ^*_{mod}, the settlement response can be fully flexible, fully rigid or somewhere in between. Clearly a more rigid response implies correspondingly smaller distortions and consequently, less damage. This highlights the potential conservativeness of assuming the building to follow the greenfield settlement.

The settlement profiles of the micro concrete and masonry buildings in tests MCS-1, MAS-1 and MAS-2, at 2% volume loss, are illustrated in Figure 8a-c respectively. Similar to STR-1, building MCS-1 is seen to respond relatively flexibly with regions of hogging and sagging evident. MAS-1 on the other hand was observed to behave relatively rigidly and simply tilted. The response of MAS-2L was found to be relatively flexible with both hogging and sagging modes of deformation observable, although the response is significantly influenced by the development of a crack above the tunnel centreline. Scatter in the settlement data for MAS-2R is observed, although the response appears to be

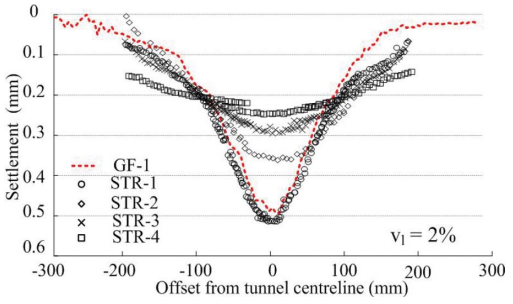

Figure 7. Surface settlement profile for structures STR-1 to STR-4.

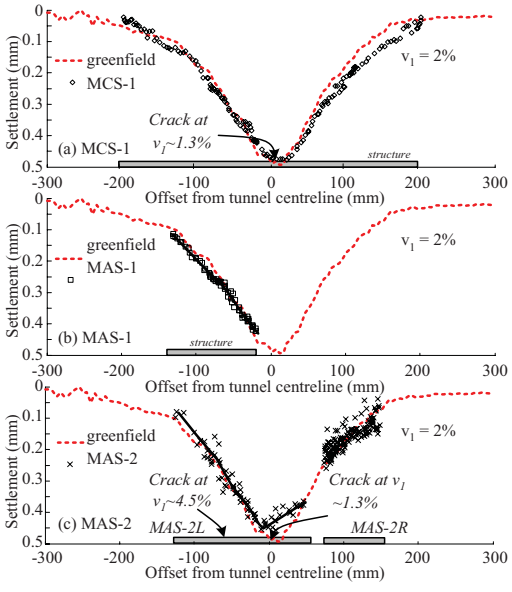

Figure 8. Building settlements compared with greenfield settlements in tests MCS-1, MAS-1 and MAS-2.

relatively flexible. Cracking and damage to buildings is discussed further in Section 5.

3.2 *Building embedment*

The settlement response of STR-4 clearly indicates that the edges of the building settle more than the greenfield trough and embed into the soil (see Figure 7). Above the tunnel centreline however, building settlements are substantially less than greenfield values, suggesting the formation of a gap between the soil and the building. The development of a gap beneath buildings STR-2 to STR-4 has been confirmed from PIV measurements (Farrell, 2010).

The formation of a gap beneath more rigid buildings is important as it results in a redistribution of the building weight away from the tunnel centreline. This trend is also evident for building MAS-1 (see Figure 8b) where building settlements

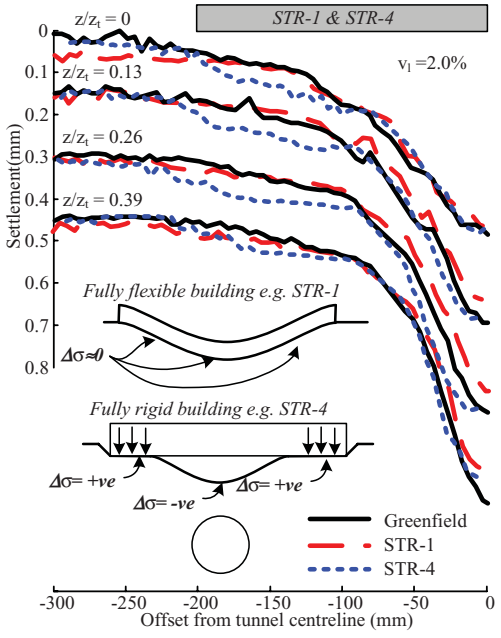

Figure 9. Settlement of soil beneath flexible and rigid buildings (STR-1 & STR-4) compared with greenfield settlements.

at the trough shoulders (~x = –80 mm) are larger than the greenfield settlements.

Figure 9 illustrates the effect of building embedment on the underlying soil through comparison of soil settlements at various depths beneath the rigid STR-4 with those beneath the flexible STR-1. The greenfield settlement profile is also shown for reference. Soil settlements beneath the flexible STR-1 are seen to agree well with greenfield values at all depths. Soil settlements beneath the rigid STR-4 however are seen to be larger than the greenfield values in the region of $-200 < x < -90$ mm, highlighting this embedment effect. The influence of this embedment beneath STR-4 is seen to extend to a depth of roughly $z/z_0 = 0.26$. This depth of influence is likely to be dependent not only on ρ^*_{mod}, but also on the building weight, as heavier buildings will redistribute more weight and cause larger settlements. Observations of building weight redistribution have been confirmed from EPC's located along the base of model buildings.

3.3 *Modification to settlement distortions*

The observed relationship between modification factors to the settlement distortions and the relative building stiffness (ρ^*_{mod}) is shown in Figure 10a and 10b for hogging and sagging distortions respectively. Design curves proposed by Franzius

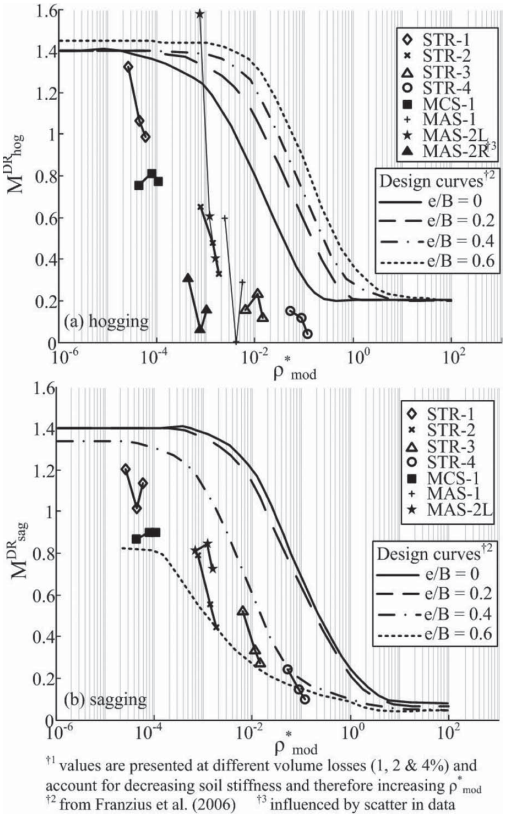

Figure 10. Modification factors in (a) hogging (b) sagging (from Franzius et al., 2006).

et al. (2006) are also shown. Measured modification factors are presented at volume losses of 1, 2 and 4% and account for the change in the soil stiffness on ρ^*_{mod}. An interesting observation is that for the very flexible STR-1, modification factors greater than unity are observed. This is consistent with observations from finite element analyses (Franzius et al, 2006) and indicates that the distortions are larger than the greenfield values. This is likely to result from the influence of horizontal shear stresses acting at the base of the building to increase the curvature.

The relationship between ρ^*_{mod} and M^{DR} is seen to be highly non-linear in both hogging and sagging which again is in agreement with observations from finite element analyses. This highly non-linear relationship is highlighted by the decrease in M^{DR} for the elastic beams (STR-1 to STR-4) as volume losses increase. This decrease in M^{DR} arises as volume losses increase soil strains which reduces the soil stiffness and increases ρ^*_{mod} which results in an increasingly rigid response. This trend is not as

evident for non elastic buildings, as cracking simultaneously reduces the building stiffness and ρ^*_{mod}.

While the agreement between the design lines and the measured M^{DR} values is relatively poor, the design lines do represent an upper bound to the modification factors, as was their intended purpose. Scatter in the modification factors—as exemplified by MAS-2L in hogging—results from the limit of the precision (0.02 mm) of PIV and the ensuing errors in estimating the deflection ratio.

4 BUILDING HORIZONTAL RESPONSE

4.1 *Horizontal displacements*

Figure 11a–c shows the horizontal displacement profile of buildings STR-4, MAS-1 and MAS-2 respectively, at 2% volume loss. Greenfield horizontal displacements are also illustrated for reference. It can be observed that STR-4 displayed negligible horizontal displacements and significantly modified the greenfield settlement profile. All buildings placed symmetrically about the tunnel centreline displayed similar behaviour.

Building MAS-1 on the other displays a net horizontal displacement which is roughly equal to the maximum greenfield horizontal displacement indicating that the ground laterally displaces the building. Differential horizontal displacements and hence horizontal strains, however, remain negligible.

A net horizontal displacement of building MAS-2L (see Figure 11c) is also observed, although the magnitude of this displacement is less than the maximum greenfield displacement. Differential horizontal displacements or horizontal strains are difficult to identify due to scatter in the data but are significantly smaller than the greenfield strains.

Horizontal displacements of building, MAS-2R are seen to agree reasonably well with the greenfield values. Despite scatter in the data differential horizontal displacements and hence horizontal strains can be observed. Horizontal strains are discussed further in Section 4.2.

Surface horizontal displacements, measured directly beneath model buildings STR-4, MAS-1 and MAS-2L at 2% volume loss, are illustrated in Figure 12a–c respectively. Greenfield horizontal displacements are also illustrated for reference. Displacements beneath STR-4 agree well with the greenfield values close to the tunnel centreline ($x > -50$ mm). Towards the edge of the building ($x < -100$ mm) friction reduces the horizontal soil displacements, indicating that where a gap does not form, horizontal soil displacements are negligible. All buildings located symmetrically about the tunnel centreline had a similar effect on the underlying soil.

The horizontal displacement of MAS-1 on the other hand is seen to cause an increase in the soil displacements towards the edge of the building

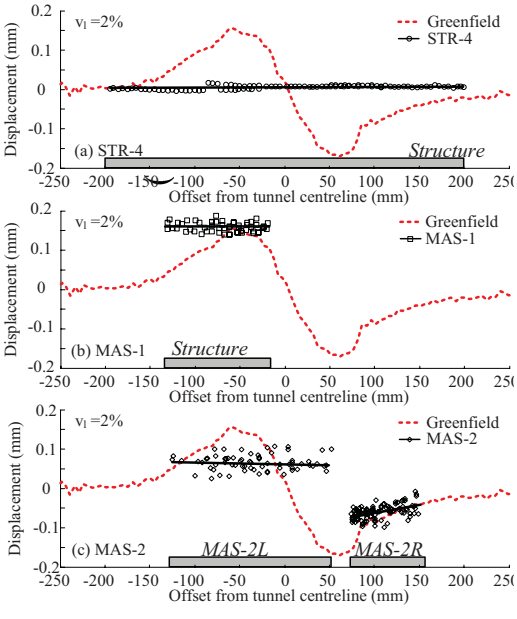

Figure 11. Horizontal displacement profile for model buildings in tests (a) STR-4, (b) MAS-1 and (c) MAS-2.

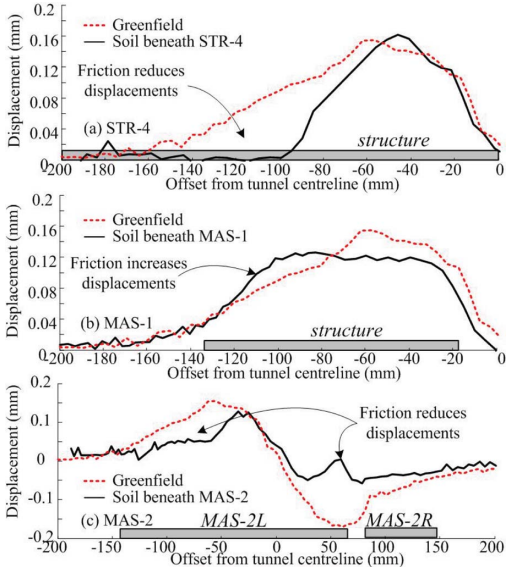

Figure 12. Horizontal displacement profile for soil beneath model buildings in tests (a) STR-4, (b) MAS-1 and (c) MAS-2.

(x < –80 mm). This also results from friction at the soil structure interface.

Similar to STR-4, MAS-2L can be seen to restrain horizontal displacements towards its edges. This is particularly evident towards the right hand side of the building (x ~ 50 mm) where large greenfield horizontal displacements (~0.2 mm) are reduced to zero. Relatively good agreement between measured horizontal displacements and greenfield displacements close to the tunnel centreline, indicate that friction in this region is significantly lower than at the edges.

4.2 *Modification to horizontal strains*

Figure 13 shows the horizontal displacements of the buildings and soil surface in test MAS-2 at a volume loss of 2%. Greenfield horizontal displacements are presented for reference. Horizontal strains, estimated from the slope of a straight line fitted to the horizontal displacements, are also indicated. Average greenfield horizontal strains across building MAS-2L are estimated as roughly 0.125%, where compression is positive. Although there is some scatter in the data, horizontal strains within MAS-2L are substantially smaller, at roughly 0.014%.This implies that strains within the building are roughly 10% of the greenfield values.

Horizontal strains within MAS-2R, however, are evident from the differential horizontal displacements and are roughly 30% of the average greenfield horizontal strain. The prototype scale axial stiffness (EA) of this building however is extremely low, due to the silica gel mortar and is equivalent to only a 4 mm thick reinforced concrete slab (for E = 27GPa). Horizontal strains within the aluminium beams tested were also found to be negligible relative to greenfield strains, as illustrated in Figure 14, for building STR-3. Similar conclusions of negligible horizontal strains being induced in buildings with continuous footings have been reached by Viggiani and Standing (2001), Mair (2003) and Dimmock & Mair (2008).

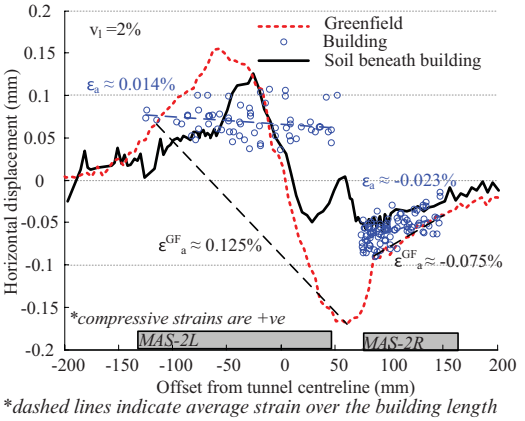

dashed lines indicate average strain over the building length

Figure 13. Estimation of horizontal strains from measured horizontal displacements of buildings in test MAS-2 and from greenfield measurements.

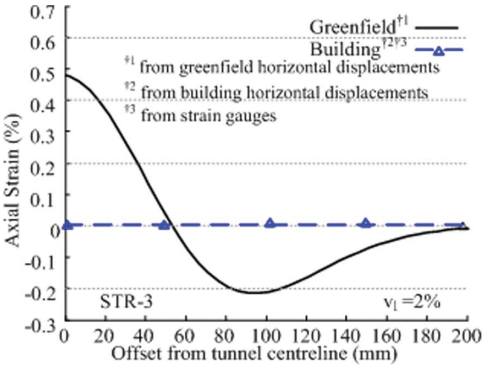

Figure 14. Measured horizontal strain in building STR-3 compared with greenfield horizontal strains.

5 DAMAGE

The development of cracks in the non elastic model buildings has been identified through an analysis of the incremental settlement profiles. Observations were later verified through visual inspection of the models. Strains at which cracking occurs have been estimated from differentiation of the settlement profile and where possible, from strain gauges.

Observed cracking in the masonry building MAS-2L is illustrated in Figure 15. Cracking in the sagging region of the trough occurred at 1.1–1.5% volume loss and at a strain of roughly 350 με. This crack developed at the base of the model, where bending induced tensile strains are largest. Cracking in the hogging region of the trough occurred at 4–5% volume loss (350–500 με) and emanated from the top of the model, again where bending induced tensile strains are largest. Cracking in building MCS-1 was also observed in the sagging region, at a volume loss of 1.3% (roughly 180 με).

A damage category chart for buildings in hogging and with an L/H ratio of 4, corresponding to STR-4, is presented in Figure 16. This chart has been developed using simple beam theory proposed by Burland and Wroth. (1974) and assuming limiting tensile strains for different damage categories as proposed by Boscardin and Cording (1989). Categories of damage, ranging from 0–5, have been defined by Burland et al. (1977) and represent an escalation from negligible damage to severe structural damage.

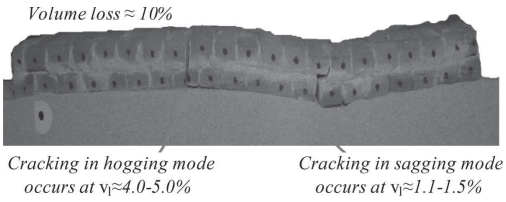

Figure 15. Observed cracking of building MAS-2 L.

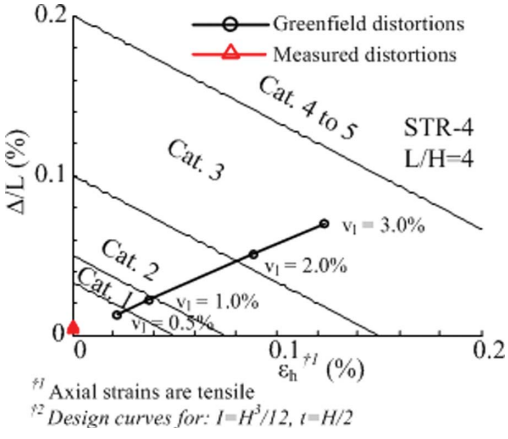

Figure 16. Damage category chart for STR-4 (L/H = 4) in hogging with greenfield and measured building distortions.

It can be observed from Figure 16 that superimposing greenfield distortions onto building STR-4 would result in category 3 level of damage, at a volume loss of 3%. However, as the building behaved rigidly and simply embedded into the soil, settlement distortions were negligible. Combined with the negligible horizontal strains, the revised risk damage can be estimated as 'negligible'. This highlights the conservativeness of assuming buildings to deform according to the greenfield distortions (both vertical and horizontal).

6 CONCLUSIONS

The response of elastic buildings and buildings capable of cracking to tunnelling induced ground movements has been investigated using centrifuge modelling. The following conclusions can be made:

1. The modification to settlement distortions is a function of both the building and soil stiffness. Results presented in this paper indicate that this relationship is highly non-linear. This agrees with finite element data in the literature (e.g. Franzius et al., 2006)
2. Buildings that respond rigidly to tunnelling do so by redistributing their weight. This can cause buildings to embed into the soil in certain places. This agrees with observations from field studies (Farrell et al., 2011).
3. Horizontal strains transferred into model buildings were generally negligible, as is often observed in the field (Mair, 2003). The exception to this was a highly flexible building which had a prototype scale axial stiffness equivalent to that of only a 4 mm reinforced concrete slab. Nevertheless, horizontal strains within this building were still less than 30% of the greenfield strains.
4. Estimating the risk of damage to buildings by superimposing greenfield distortions can be highly conservative due to the influence of the soil-structure interaction on the settlement and particularly the horizontal building distortions. Centrifuge test results have shown that this interaction can be roughly quantified from empirical relationships, such as those proposed by Franzius et al. (2006)

ACKNOWLEDGEMENTS

The authors would like to thank the EPSRC and the Cambridge European Trust for funding this research.

REFERENCES

Boscardin, M.D. & Cording, E.J. (1989). Building response to excavation-induced settlement. *ASCE Journal of Geotechnical Engineering,* 115, pages 1–21.

Burland, J.B., Broms, B.B. & De Mello, V.F.B. (1977). Behaviour of foundations and structures. *Proceedings of the 9th International Conference on Soil Mechanics and Foundations Engineering*, volume 2, pages 495–546. Tokyo.

Burland, J.B. and C.P. Wroth (1974). Settlement of buildings and associated damage. *Settlement of Structures*, Cambridge, pages 611–654. Pentech Press, London, Cambridge.

Dimmock, P.S. and R.J. Mair (2008). Effect of building stiffness on tunnelling-induced ground movement. *Tunnelling and Underground Space Technology*, 23, no. 4, pages 438–450.

Farrell, R.P., Mair, R.J., Sciotti, A., Pigorini, A. & Ricci, M. (2011). The response of buildings to tunnelling: a case study. *Geotechnical Aspects of Underground Construction in Soft Ground.* Unpublished. Rome. Balkema.

Franzius, J.N., Potts, D.M. & Burland, J.B. (2006). The response of surface structures to tunnel construction. *Proceedings of the Institution of Civil Engineering—Geotechnical Engineering*, 159, no. 1, pages 3–17.

Mair, R.J (2003). Research on tunnelling-induced ground movements and their effects on buildings—lessons from the Jubilee Line Extension. *Response of buildings*

to excavation induced ground movements. Proceedings of the international conference, pages 3–26, CIRIA SP199.

Mair, R.J., Taylor, R.N. & Burland, J.B. (1996). Prediction of ground movements and assessment of risk of building damage due to bored tunnelling. *Geotechnical Aspects of Underground Construction in soft ground*, pages 713–718. Balkema, London.

Mair, R.J. & Taylor, R.N. (2001). Settlement predictions for Neptune, Murdoch and Clegg Houses and adjacent masonry walls. Building Response to tunnelling–Case studies from construction of the Jubilee Line Extension, London. Vol. 1: Projects and Methods. In Burland J.B., Standing J.R., and Jardine F.M., (eds) *CIRIA SP200*, pages 217–228. London: Thomas Telford.

Marshall, A.M. (2009). Tunnelling in sand and its effect on pipelines and piles. *Ph.D. thesis*, Cambridge University, UK.

Potts. D.M. & Addenbrooke, T.I. (1997). A structures influence on tunnelling induced ground movements. *Proc. Inst. Civ. Engrs. Geotechnical Engineering*, Vol. 125, pages 109–125.

Taylor, R.N. (1995). Geotechnical Centrifuge Technology. London: Blackie Academic and Professional.

Taylor, R.N. & Grant R.J. (1998). Centrifuge modelling of the influence of surface structures on tunnelling induced ground movements. In Negro Jr & Ferreira (eds). *Tunnels and Metropolises.* Pages 261–265. Rotterdam: Balkema.

Viggiani, G. & Standing, J.R. (2001). The Treasury. *In:* Burland, J.B., Standing, J.R. & Jardine, F.M. (eds.) *Building response to tunnelling: case studies from construction of the Jubilee Line Extension, London*, pages 351–366. London, volume 2. CIRIA and Thomas Telford.

White, D.J., Take, W.A. & Bolton, M.D. (2003). Soil deformation measurement using particle image velocimetry (PIV) and photogrammetry. *Geotechnique*, Vol. 53(7), pages 619–631.